

Refine and Represent: Region-to-Object Representation Learning

Akash Gokul^{1*}, Konstantinos Kallidromitis^{2*}, Shufan Li^{1*},
Yusuke Kato³, Kazuki Kozuka³, Trevor Darrell¹, Colorado J Reed¹

¹Berkeley AI Research

²AI Lab, Panasonic R&D Company of America

³Digital and AI Technology Center, Technology Division, Panasonic Holdings Co.

{akashgokul, jacklishufan}@berkeley.edu, k.kallidromitis@us.panasonic.com

Abstract

Object-centric self-supervised learning methods have recently led to state-of-the-art results on dense prediction tasks such as object detection and segmentation. However, object-centric pretraining methods rely on fixed, off-the-shelf segmentation heuristics to identify objects in an image. In this paper, we present Region-to-Object Representation Learning (R2O), which oscillates between predicting segmentation masks and using these masks to pretrain an encoding network. R2O determines the segmentation masks by clustering encoded features. R2O then pretrains an encoding network by performing region-to-region similarity learning, where the encoding network takes different views of an image and maps the segmented areas to similar encoded features. R2O uses a region-to-object pretraining curriculum which encourages the predicted segmentation mask to output a large number of regions early on and progressively fewer regions throughout training, which as we show, corresponds to a region-to-region and then object-to-object pretraining. Representations learned using R2O lead to state-of-the-art transfer performance for object detection and instance segmentation, and semantic segmentation. Additionally, R2O ImageNet pretrained models are able to surpass state-of-the-art in unsupervised object segmentation on the Caltech-UCSD Birds 200-2011 dataset without further training.

1. Introduction

Progress in self-supervised pretraining in computer vision has led to improvements on a wide range of transfer learning tasks such as image classification, object detection, and semantic segmentation [6, 8, 25, 26, 28]. Instance

*Denotes co-first authorship where co-first authors can prioritize their names in their resumes/websites.

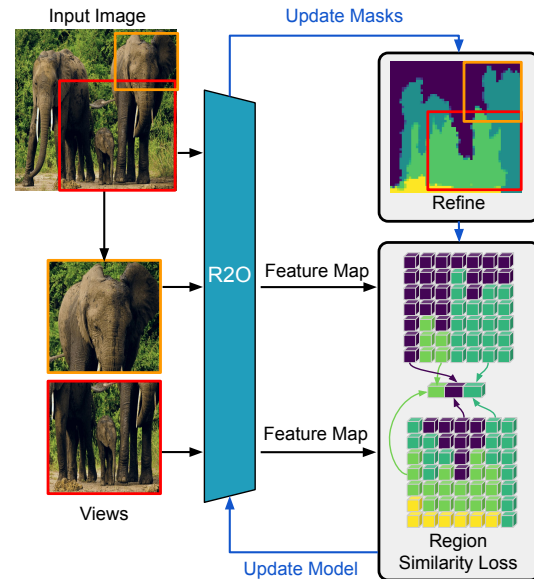


Figure 1. **R2O unifies region-based and object-centric self-supervised learning by jointly learning to discover and represent regions and objects.** Previous object-centric pretraining methods use off-the-shelf segmentation priors to learn object-centric representations. In contrast, R2O learns object-centric representations by oscillating between predicting a segmentation mask (that depends on the representations) and training representations (using the segmentation mask). Specifically, R2O pools features corresponding to segmented regions (region similarity loss) and enforces representation similarity for those features across views. Learned representations then lead to improved, increasingly object-centric masks, which in turn, lead to improved representations.

discrimination pretext objectives have driven many of these advancements, whereby contrasting augmented views of an input image, a network learns representations that are in-

variant to predefined image-level data augmentations. However, much of this work has focused on scene-level pretraining, which as recent works have shown, is not optimal for pixel-level prediction tasks, such as semantic segmentation [31, 60, 67].

In order to train features which are better suited for dense prediction tasks, recent works have proposed extensions to the image-level pretraining objective. These approaches can be categorized into two types: region-based or object-centric. Region-based pretraining [46, 60, 64, 68] enforces predictive invariance between image patches, *i.e.* regions, which are present in two views of an image. Thus, region-based methods can learn from all overlapping regions, regardless of size or content. While region-based methods outperform image-level pretraining methods on pixel-level prediction tasks, object-centric pretraining methods have led to better results [2, 31, 52, 57, 66, 69].

Object-centric pretraining uses segmentation heuristics to localize objects and enforces representational invariance to the features corresponding to those objects. In particular, DetCon [31] presents a simple, state-of-the-art approach which uses static object masks, generated by an off-the-shelf segmentation heuristic, in order to train object-centric features. However, because object-centric pretraining methods rely on off-the-shelf segmentation masks that are fixed throughout pretraining, their performance is limited by the accuracy of their object prior. In this paper, we seek an object-centric pretraining approach that does not rely on heuristics to localize objects but can instead discover object-centric regions while learning to represent them.

We present Region-To-Object representation learning (*R2O*): a framework that learns region-based and object-centric features by evolving predicted segmentation masks throughout pretraining and encouraging representational similarity for the features corresponding to the contents of the predicted mask. *R2O* uses a *mask prediction module* to transform multiple small-scale image regions into larger object-centric regions using learned features. Over the course of pretraining, predicted masks are used to learn representations which in turn leads to more accurate, object-centric segmentations in future epochs (see Fig. 1). This enables *R2O* to train object-centric features without relying on segmentation heuristics.

Furthermore, we find that pretraining for dense prediction tasks benefits from both region-based and object-centric objectives at different stages of the pretraining process. Thus, we introduce a region-to-object curriculum, which gradually reduces the number of segments within predicted masks, in order to encourage region-level pretraining, corresponding to small image regions, early on and increasingly object-centric representation learning as pretraining progresses. This curriculum enables *R2O* to incorporate the strengths of region-based and object-centric

pretraining as earlier epochs leverage a large number of image patches to train local features, as seen in region-based methods, and the later epochs train the object-centric features which are important for downstream tasks.

We study *R2O* on a range of datasets and tasks, including object detection, instance segmentation, and semantic segmentation. Our contributions are summarized as follows:

- We present *R2O*: a self-supervised pretraining method that learns region-based and object-centric representations by predicting a segmentation mask, using learned image features, and learning representations of the contents within the mask.
- We introduce a region-to-object pretraining curriculum for *R2O* that begins by training local features corresponding to simple image regions, *e.g.* adjacent pixels sharing similar color values, and gradually progresses to learn object-centric features.
- *R2O* pretraining improves transfer performance from ImageNet in object detection and instance segmentation on MS COCO $1\times$ (+0.2 AP^{bb}, +0.3 AP^{mk}) and $2\times$ (+0.9 AP^{bb}, +0.4 AP^{mk}), and semantic segmentation for PASCAL VOC (+1.3 mIOU) and Cityscapes (+0.3 mIOU) when compared to previous methods. After pretraining on COCO, *R2O* outperforms earlier methods by +1.9 mIOU for PASCAL VOC and +2.4 mIOU for Cityscapes. Additionally, *R2O* further improves state-of-the-art unsupervised segmentation performance on Caltech-UCSD Birds 200-2011 (CUB-200-2011) by +3.3 mIOU *despite not finetuning on CUB-200-2011*.

2. Related Works

Image-Level Self-Supervised Pretraining Self-supervised learning aims to learn representations from unlabelled data in such a way that they are informative and effective when transferred to downstream tasks [3]. Early works in discriminative visual representation learning focused on training encoders to predict the position of an image patch [18, 45], predict the angle of rotation [23], and predict the colors in a grayscale image [72]. Current methods have shifted to training an encoder to learn representations that are invariant to data augmentations [6, 8, 10, 25, 28, 44, 49]. This form of pretraining, known as instance discrimination, is often achieved through contrastive learning [47] or a teacher-student dual-network [25]. The contrastive objective encourages representations from the same image to be invariant to data augmentations and dissimilar to representations from other images (commonly referred to as negatives). On the contrary, Siamese representational learning methods do not rely on negatives. [10, 25].

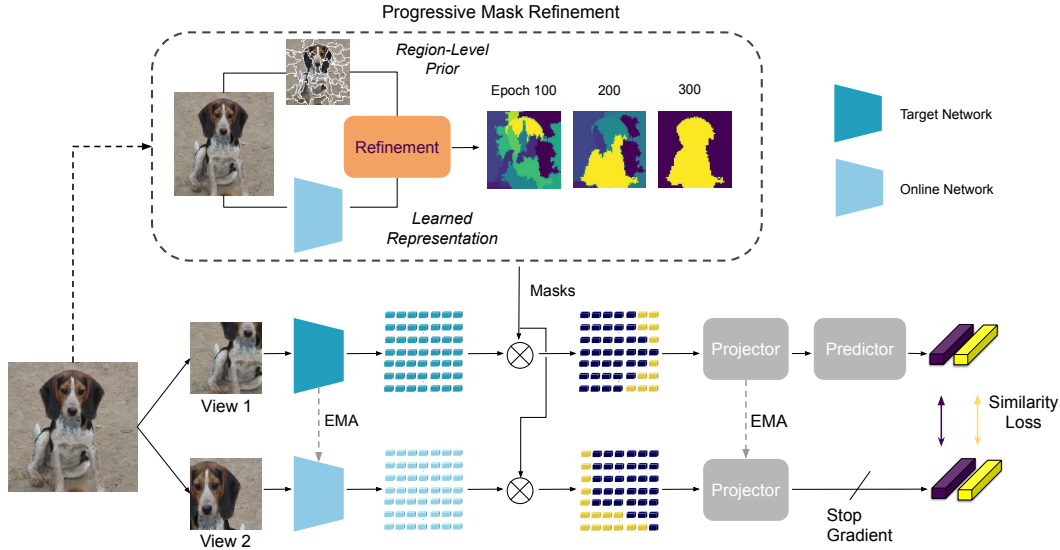


Figure 2. **The R2O architecture.** R2O consists of two interdependent steps: (1) *Mask Prediction*, where small image regions (given by a region-level prior) are transformed into object-centric masks using learned features and (2) *Representation Learning*, where object-level representations are learned. Step 1 produces object-centric segmentations by computing features for each region given by the region-level prior and performing K-means clustering on these region-level embeddings. Step 2 encourages representation similarity for the features corresponding to the contents of the mask in each view. Through this process, we have found that the features learned through the second step lead to increasingly object-centric segmentations which in turn train object-centric representations. Given the importance of region-level features in our mask prediction process, R2O employs a region-to-object curriculum which gradually decrease the number of clusters (K) during mask prediction from a very high value ($K = 128$) to a low value ($K = 4$), which as we show, enables region-based pretraining early on during training and slowly evolves to object-centric pretraining. We denote online and target network as ON, TN respectively.

Region-Based and Object-Centric Self-Supervised Pretraining

Instance discrimination pretraining has primarily focused on learning image-level representations. While this is suitable for scene-level downstream tasks such as classification, it does not explicitly learn the locality of features which is critical for tasks such as object detection and semantic segmentation. Recent works [2, 46, 60, 61, 64, 65, 67, 68] have extended the instance discrimination paradigm to also learn region-based features. These methods enforce representational invariance to image regions in different views without taking into consideration the content in these regions. Examples include DenseCL [60], which trains local features to be invariant across views while also performing the standard image-level representation training, and ReSim [64], which performs region-level representation learning by sliding a window across the image regions present in both views and enforcing region-based representational similarity. Our work extends region-based pretraining by first training region-level features and gradually discovering object-centric segmentations which eventually train object-centric features.

Concurrent to this line of work are methods [2, 31, 52, 57, 61, 66, 69] that use heuristics [21, 54] to locate objects and enforce representational invariance for the features corresponding to these objects. The closest related work is

DetCon [31], which uses unsupervised segmentation algorithms to train object-level representations. In contrast, our method is able to discover and represent objects by evolving region-level segmentations into object-centric masks using learned features. Other works in this area [2, 57, 61, 69] focus on training object-centric features for a specific task, such as object detection, and do not train a network to learn features that can transfer to multiple tasks. Concurrent works such as Odin [31] and SlotCon [62] have proposed object-level pretraining methods which do not rely on segmentation heuristics but instead use learned features to segment the input image. Similar to Odin, R2O uses K-means clustering on image features to help discover object-like regions. However, unlike Odin or SlotCon which focus on only training object-level features, R2O pretraining involves training both local features and object-level features.

Region Clustering

In this work, we use clustering to refine small image regions into object-centric masks. Clustering has a long history in unsupervised semantic segmentation [1, 13, 14, 17, 21, 33]. This trend has continued in the era of deep learning. Current methods utilize clustering assignments in order to learn spatially and semantically consistent embeddings [12, 34, 36, 37]. For example, one

popular approach [34, 37] involves training pixelwise embeddings by clustering these embeddings and using the cluster assignments as pseudo labels. Other works [12, 36] train embeddings using a similarity loss and task-specific data augmentations. Our work does not focus on the task of unsupervised semantic segmentation, but instead, focuses on using clustering to localize objects for learning transferable representations. Our method uses K-means clustering [39] because of its simplicity and effectiveness.

3. Method

We present *R2O*, a self-supervised pretraining method that enables region-level and object-centric representation learning. At a high level, *R2O* transforms region-level image priors into object-centric masks through a *mask prediction module* and encourages representational invariance for the features corresponding to the contents of the discovered masks (see Fig. 2). The training process uses a simple region-level prior, such as SLIC [1], to generate a fixed set of fine-grained image regions. During pretraining, features for each region are pooled and clustered using K-means to create segmentation masks. A high number of clusters, K , leads to masks that group small image regions together. Conversely, we have found that using a lower number of clusters leads to semantically meaningful segmentations which tend to correspond to objects. *R2O* then promotes representational similarity for the features corresponding to the predicted masks, by aligning said features across different views of an image. Finally, our region-to-object curriculum enables region-level and object-centric representation learning by gradually progressing masks from regional fragments to object-centric segmentations.

Formulation We formulate the pretraining objective as a bilevel optimization problem. In this formulation, the upper-level objective transforms a region-based prior into an object-centric mask (Sec. 3.1) and the lower-level objective optimizes representational invariance for mask-level features (Sec. 3.2). Let X refer to a given image and R be the region-level prior for the image (e.g. SLIC superpixels). The outer loop computes a cluster assignment, M , which is used to segment the image X , according to a mask-level objective ($\mathcal{L}_{\text{mask}}$) given the representation $f_{\theta}(X)$ and the region-level prior R (Eq. (1)). The inner loop optimizes the parameters, θ , of the encoder, f_{θ} , following any representation learning objective ($\mathcal{L}_{\text{repr}}$) with respect to the segmentations created using M (Eq. (2)).

$$\min_M \mathcal{L}_{\text{mask}}(M; f_{\theta^*}(X), R) \quad (1)$$

$$\text{s.t. } \theta^* = \underset{\theta}{\operatorname{argmin}} \mathcal{L}_{\text{repr}}(f_{\theta}(X); M) \quad (2)$$

3.1. Object-Centric Segmentation via Mask Prediction

Our *Mask Prediction* step discovers object-centric segmentations by clustering region-level features for regions given by a region-level prior, such as SLIC superpixels [1]. Specifically, we define an object-centric segmentation as a set of clusters, M , which satisfy criteria such as color consistency, spatial proximity, and representational similarity. Region-level priors provide segmentations which satisfy image-level criteria, such as color consistency, and can be derived solely from a given image. These region-level priors are fixed during training and add negligible overhead as they can be generated prior to pretraining. However, as illustrated in Figure 2, these simple region-level priors do not accurately segment objects in the scene, but rather, group together small neighboring regions. In order to transform our region-level prior into an object-centric segmentation, we build upon recent works, which show that representations learned during self-supervised pretraining can encode object-level semantics [56, 66, 71], and incorporate learned features as part of our mask prediction step.

We approximate the solution to the upper-level optimization problem (Eq. (1)) by performing K-Means clustering on the set of region-level image features. For each region from our region-level prior, we compute an embedding, p_i , using a mask-pooling operation, where each region has a binary mask that selects the corresponding features in the convolutional feature map. This generates a set of region-level embeddings $P = \{p_1, \dots, p_{|R|}\}$ where $|R|$ is the number of distinct regions generated by the region-level prior R . Next, we apply K-Means clustering to the region-level embeddings in P in order to compute clusters $M = \{M_1, \dots, M_K\}$ (Eq. (3)). Below, we denote $|M_i|$ as the number of points assigned to cluster M_i and μ_i is the mean of the points in M_i . Given cluster assignments M , we produce an object-centric segmentation, m , by assigning each pixel in the representation $f_{\theta}(X) \in \mathbb{R}^{H \times W \times D}$ to its nearest cluster center (see Mask in Fig. 2).

$$\mathcal{L}_{\text{mask}}(M; f_{\theta}(X), R) = \frac{1}{K} \sum_{k=1}^K \frac{1}{|M_k|} \sum_{p \in M_k} \|p - \mu_k\|^2 \quad (3)$$

3.2. Object-Centric Representation Learning

Our representation learning process follows the BYOL objective [25]. Since optimizing this inner objective to convergence can be expensive, we approximate θ^* by minimizing $\mathcal{L}_{\text{repr}}(f_{\theta}(X); M)$ for one step using mini-batch gradient descent.

Setup Given an image X , we create two views: $x_1 = \mathcal{T}_{\text{aug}}(X)$, $x_2 = \mathcal{T}_{\text{aug}}(X)$, where \mathcal{T}_{aug} is any image augmentation policy. We use m to obtain m_1, m_2 corresponding to

views x_1, x_2 . Further, we use a Siamese architecture with two similar networks: an online encoder f_θ (denoted by parameters θ) and a target encoder f_ξ (denoted by parameters ξ). The target network is updated using an exponential moving average of the online network’s parameters.

Pretraining We begin by computing $f_\theta(x_1), f_\xi(x_2) \in \mathbb{R}^{H \times W \times D}$. Next, we replace the commonly used global-pooling with mask-pooling. This operation generates the average embeddings within the view-specific masks m_1 and m_2 . We compute $h_{\theta,1}$ and $h_{\xi,2}$ by applying mask-pooling to $f_{\theta,1}$ and $f_{\xi,2}$. Following the Siamese architecture, we compute $z_{\theta,1}$ and $z_{\xi,2}$ by forward-passing $h_{\theta,1}, h_{\xi,2}$ through the online network’s projector and the target network’s projector respectively. Finally, we forward-pass $z_{\theta,1}$ through the online network’s predictor to obtain $q_\theta(z_{\theta,1})$. We adopt the L2 loss according to the BYOL architecture (Eq. (4)). To make this loss symmetric for the view, we perform the same computation after swapping the two views to obtain $z_{\theta,2}, z_{\xi,1}$. Our final loss is provided in Equation (5).

$$\mathcal{L}_{\text{BYOL}}(z_\theta, z_\xi) = 2 - 2 \cdot \frac{q_\theta(z_\theta) \cdot z_\xi}{\|q_\theta(z_\theta)\|_2 \cdot \|z_\xi\|_2} \quad (4)$$

$$\mathcal{L}_{\text{repr}} = \mathcal{L}_{\text{BYOL}}(z_{\theta,1}, z_{\xi,2}) + \mathcal{L}_{\text{BYOL}}(z_{\theta,2}, z_{\xi,1}) \quad (5)$$

3.3. Region-to-Object Curriculum

Empirically, we have found that varying the number of segments in the predicted masks, from a high number to a low number, results in improved downstream performance and more accurate masks. Thus, we introduce a region-to-object curriculum which allows for *R2O* pretraining to learn both region-based and object-centric features. Specifically, we control the number of clusters K introduced in the mask prediction step (Sec. 3.1). We have found that a region-to-object curriculum where K begins at a high value, *e.g.* $K = 128$, and is reduced to a low value, *e.g.* $K = 4$, over pretraining works best in terms of downstream performance. In the Appendix (Fig. 5), we provide a visualization of the masks predicted during pretraining in order to illustrate how this curriculum allows for predicted masks to become increasingly object-centric.

4. Results

We evaluate *R2O* via common transfer learning paradigms by pretraining using the images in the train set of the ImageNet ILSVRC-2012 dataset [51]. We evaluate representations when finetuned for object detection and instance segmentation on MS COCO [38] and semantic segmentation on PASCAL VOC [20] and Cityscapes [16]. We also explore pretraining on scene-centric data and provide

experiments which evaluate transfer performance after pre-training using MS COCO `train2017`. Additionally, we investigate performance on unsupervised object segmentation for Caltech-UCSD Birds 200-2011 [59] when using our ImageNet pretrained models. Lastly, we perform several ablations exploring the various formulations and implementation specifics of *R2O*. Unless otherwise stated, results for existing methods are computed using pretrained weights officially released by the authors. The license, PII, and consent details of each dataset are in the respective papers. The code and models used in this work will be made publicly available.

Architecture We use a ResNet-50 [30] architecture for all encoders in order to enable fair comparison with prior works. In the Appendix, we explore using a Vision Transformer (ViT) encoder [19]. Following BYOL, all projector and predictor heads are 2 layer MLPs which use batch normalization [35] after the hidden layer. Our mask prediction step uses the C4 output from our target network. For efficiency purposes, we perform K-means over the mini-batch on each GPU. Our predicted mask m is of shape (14, 14). We use RoIAlign [29] to align m with views x_1 and x_2 . Our region-to-object representation learning step applies mask-pooling to the C5 output of the ResNet-50 similar to the existing use of global pooling.

Optimization We follow the optimization details of BYOL (full details in Appendix). Specifically, we use a base learning rate of 0.3, which is scaled linearly to the product of the batch size and K , and a weight decay of 10^{-6} . The learning rate is decayed by a cosine schedule after a warmup period which is one percent of the total pre-training time, *e.g.* 300 epochs of pretraining uses 3 warmup epochs. Our target network’s parameter τ , used in the exponential moving average (EMA), is increased over training following a cosine schedule. We use the LARS optimizer with a global batch size of 4096 distributed over 128 NVIDIA V100 GPUs using PyTorch 1.10 [48].

Mask Prediction We precompute 100 regions for each image using SLIC. We use a cosine scheduler that decreases the value of K , used in K -means, from 128 to 4 over the course of training. See Appendix for details.

4.1. Transfer Learning Details

Object Detection and Instance Segmentation: MS COCO We finetune our encoder as the backbone of a Mask-RCNN (R50-FPN) [29] using Detectron2 [63]. We follow the $1 \times$ (12 epochs) and $2 \times$ (24 epochs) training schedule, training on MS COCO’s `train2017` dataset and evaluating on the `val2017` dataset. We report average

Method	COCO 1×		COCO 2×		PASCAL VOC	Cityscapes
	AP ^{bb}	AP ^{mk}	AP ^{bb}	AP ^{mk}		
Supervised	38.9	35.4	40.6	36.8	72.4	74.7
MoCo v2 [9]	38.9	35.4	40.9	37.0	73.9	75.6
BYOL [†] [25]	40.6	37.5	42.0	38.7	75.0	75.8
DenseCL [60]	40.3	36.4	41.2	37.3	73.8	76.1
ReSim [64]	39.3	35.7	41.1	37.1	74.3	75.5
PixPro [67]	41.4	-	-	-	74.2	75.9
DetCon _B [†] [31]	41.5	38.0	42.1	38.9	76.0	76.2
DetCo [65]	39.4	34.4	41.4	35.8	74.3	74.9
SlotCon [*] [62]	41.3	37.8	42.9	39.3	76.2	76.1
<i>R2O</i>	41.7	38.3	43.0	39.3	77.3	76.6

Table 1. Performance on COCO object detection and instance segmentation, and semantic segmentation for PASCAL VOC and Cityscapes following ImageNet pretraining. All methods pretrained a ResNet-50 backbone and finetune a Mask-RCNN (R50-FPN) for COCO and a FCN for PASCAL VOC and Cityscapes. *: Denotes concurrent work. †: Results from re-implementation.

precision for bounding box predictions (AP^{bb}) and mask predictions (AP^{mk}). Further details such as variance across multiple random seeds are reported in the Appendix.

Semantic Segmentation: PASCAL VOC and Cityscapes

We evaluate our semantic segmentation performance by finetuning the encoder as the backbone of a FCN [40] using MMSegmentation [15]. For PASCAL VOC, we finetune using the `train_aug2012` dataset for 45 epochs. For Cityscapes, we finetune using the `train_fine` dataset for 160 epochs. Our evaluation pipeline follows the architecture and hyperparameters reported by the authors of MoCo [28]. Performance is measured by mean intersection-over-union (mIOU) on `val2012` and `val_fine` respectively.

4.2. ImageNet-1K Transfer

We use the BYOL data augmentation policy to generate two views during pretraining which lasts for 300 epochs.

Object Detection and Instance Segmentation

Table 1 shows our performance on COCO object detection and instance segmentation. *R2O* outperforms prior methods when using the 2× schedule (+0.9 AP^{bb}, +0.4 AP^{mk}) and is competitive with these methods when using the 1× schedule (+0.2 AP^{bb}, +0.3 AP^{mk}). When compared to concurrent work (SlotCon), *R2O* demonstrates an improvement of +0.4 AP^{bb} and +0.5 AP^{mk} when using the 1× schedule. We attribute our state-of-the-art performance on instance segmentation to the nature of our pretraining. *R2O* segments a scene by refining a large number of small image regions into a few larger regions that are semantically meaningful while learning representations corresponding to each of the discovered segments. Thus, segmentation-based tasks

should benefit from this form of pretraining as representations learned during pretraining rely upon the boundaries of discovered masks instead of rectangular bounding boxes.

Semantic Segmentation

As seen in Table 1, we outperform previously existing methods on PASCAL VOC (+1.3 mIOU) and Cityscapes (+0.3 mIOU) semantic segmentation. Compared to concurrent work (SlotCon), *R2O* provides an improvement of +1.1 mIOU and +0.5 mIOU on PASCAL VOC and Cityscapes respectively. We believe our improvements in semantic segmentation demonstrate the benefits of pretraining region-level and object-centric representations. *R2O* improves transfer performance on this task as pixel-level features are learned while also training the object-centric representations needed to identify the objects in the scene. In particular, the benefits of *R2O* is demonstrated by our state-of-the-art performance on the PASCAL VOC semantic segmentation task, a pixel-level classification task which is object-focused as most of its classes are also present in ImageNet-1K.

4.3. COCO Transfer

We further explore using *R2O* when training on COCO, a scene-centric dataset. In comparison to the curated, object-centric benchmark of ImageNet pretraining, COCO images often contain multiple objects. Thus, scene-centric datasets such as COCO provide a challenging benchmark for object-centric pretraining as they test the effectiveness of object discovery methods and the generalizability of the pretraining method. For these reasons, pretraining on scene-centric data has recently become an important benchmark in self-supervised learning [31, 55, 60, 66]. We perform an additional experiment to evaluate the transfer performance after pretraining on COCO `train2017`. We use the same

Method	PASCAL VOC	Cityscapes
MoCo v2 [9]	69.2	73.8
DenseCL [60]	68.5	74.0
DetCon _B [†] [31]	72.4	73.7
SlotCon [*] [62]	74.3	76.0
<i>R2O</i>	74.3	76.4

Table 2. **Performance on PASCAL VOC and Cityscapes semantic segmentation (mIOU) following COCO pretraining.** After pretraining on scene-centric data, *R2O* demonstrates state-of-the-art transfer performance for semantic segmentation on PASCAL VOC and Cityscapes. *: Denotes concurrent work. †: Results from re-implementation.



Figure 3. **Visualization of masks predictions during COCO pretraining.** In the later epochs of pretraining, *R2O* predicted masks are able to discover object-centric regions even in multi-object, scene-centric datasets such as COCO.

architecture, hyperparameters, and region-to-object schedule, *i.e.* $K = 128 \rightarrow K = 4$, as detailed in our ImageNet-1K experiments. We evaluate transfer performance for semantic segmentation on PASCAL VOC and Cityscapes following the details in Sec. A.2. As seen in Table 2, *R2O* outperforms prior methods when pretrained on scene-centric data by +1.9 mIOU on PASCAL VOC and +2.4 mIOU on Cityscapes while being competitive with the concurrent work of SlotCon. We have also found the quality of *R2O* predicted masks to be comparable to those generated during ImageNet pretraining when measuring average best overlap (ABO) [54]. Specifically, at the end of pretraining, *R2O* predicted segmentations obtain 0.46 ABO when pretraining on COCO and 0.49 ABO when pretraining on ImageNet.

Method	CUB
<i>Self-Supervised Pretraining Methods</i>	
MoCo v2 [9]	63.5
BYOL [†] [25]	65.1
<i>Unsupervised Object Segmentation Methods</i>	
PerturbGAN [5]	38.0
ReDO [7]	42.6
OneGAN [4]	55.5
Voynov <i>et al.</i> [58]	68.3
Melas <i>et al.</i> [43]	66.4
<i>R2O</i>	71.6

Table 3. **Performance on CUB-200-2011 segmentation.** Results report the mean intersection-over-union (mIOU) for foreground-background segmentations of images in the Caltech-UCSD Birds 200-2011 (CUB-200-2011) test set. Interestingly, we are able to outperform existing methods [4, 5, 7, 58], *without finetuning our ImageNet pretrained encoder.* †: Results from re-implementation.

4.4. Unsupervised Object Segmentation

We investigate the quality of segmentations from *R2O* pretrained features by evaluating unsupervised object segmentation on Caltech-UCSD Birds 200-2011 (CUB-200-2011). We use our ImageNet pretrained ResNet-50 and generate object segmentations by applying K-means clustering to image features with $K = 5$. We use Hungarian matching to assign one segment as the foreground and the remaining segments are considered as background. This approach accounts for the high variance in the background (*e.g.* trees, ground, sky, etc.). Table 3 shows our performance, measured by mean intersection-over-union (mIOU), when segmenting the foreground and background on a test set from CUB-200-2011 used in prior works [7]. Table 3 also provides baselines using self-supervised pretrained methods, such as MoCo v2 [9] and BYOL [25], following our evaluation protocol. In comparison to existing unsupervised object segmentation methods [4, 5, 7, 58], segmentation via K-means clustering of *R2O* pretrained ResNet-50 features surpasses state-of-the-art (+3.3 mIOU) *without finetuning on CUB-200-2011*. Similar to our protocol, Melas *et al.* [43] extract accurate segmentations from ImageNet pretrained GANs, without finetuning on CUB-200-2011, in order to train a UNet [50]. *R2O* outperforms the work of Melas *et al.* (+5.2 mIOU) using only K-means clustering on features from *R2O* pretrained encoders. We provide visualizations of *R2O* segmentations in the Appendix.

4.5. Ablation and Analysis

To examine the importance of the components within the *R2O* architecture, we perform ablation experiments to determine the importance of the mask prediction module,

Mask Prediction	SLIC Prior	Region-to-Object Schedule	PASCAL VOC	ImageNet-100
✗	✗	✗	66.4	69.0
✗	✓	✗	67.0	69.0
✓	✗	✗	69.0	74.1
✓	✗	✓	68.7	77.6
✓	✓	✗	68.8	75.7
✓	✓	✓	72.1	85.5

Table 4. **Importance of *R2O* components.** We ablate the key components of *R2O*, namely: the mask prediction module, the use of a prior (SLIC), and the region-to-object schedule. We evaluate performance on PASCAL VOC semantic segmentation (mIOU) and k -NN classification (%) on ImageNet-100. As shown, the combination of using Mask Prediction, SLIC Prior, and Region-to-Object Schedule is necessary for the top performing result (62.3 mIOU) – removing any component affects performance by at least -2.6 mIOU and -5.1% .

SLIC prior, and region-to-object curriculum. The models used in these ablations are pretrained on ImageNet-100 [53] for 300 epochs and evaluated on PASCAL VOC semantic segmentation and ImageNet-100 classification using k -nearest neighbors. We provide ablations on the effect of the type of scheduler used for our region-to-object curriculum (*e.g.* cosine, linear), the type of pretraining curriculum (fixed K , object-to-region, region-to-object) and type of region-level prior (SLIC versus spatial segmentation) in the Appendix. The Appendix also explores using a contrastive representation learning objective.

Effect of Mask Prediction and Region-to-Object Pretraining. Table 4 details the results of ablating each key component in *R2O* pretraining. The baseline method, which is a simple region-based pretraining method that does not use a SLIC prior, region-to-object schedule, nor the mask prediction module, performs the worst. The impact of the region-to-object curriculum on PASCAL VOC performance is similar to that of the SLIC prior (+3.3 mIOU versus +3.4 mIOU). However, the larger impact of the region-to-object curriculum on the k -NN evaluation (+9.8% versus +7.9%) suggests that the region-to-object pretraining curriculum is the most important component, followed by the SLIC region-level prior. These findings can be justified by the architecture of our mask prediction module which relies on region-level features in order to discover larger object-centric regions.

Comparison with Odin [31]. While we are unable to fairly compare with performance reported by Odin, due to their significantly longer pretraining schedule, we have re-implemented their method and pretrained Odin on ImageNet-100. *R2O* outperforms Odin by +3.1 mIOU for semantic segmentation on PASCAL VOC (72.1 mIOU versus 69.0 mIOU) when both methods are pretrained on ImageNet-100. It should be noted that the authors of Odin did not provide publicly available code or weights.

Intuitions on *R2O*’s effectiveness. In line with findings from previous work in object-centric pretraining, we have found that *R2O* learns to discover and represent semantically meaningful regions which tend to correspond to objects. *R2O* predicted masks segment object-centric regions but these segmentations may contain artifacts such as failing to distinguish different objects (see Appendix). These artifacts are also exhibited by off-the-shelf segmentation heuristics used in previously state-of-the-art object-centric pretraining methods, and thus highlight the effectiveness of learning to represent object-centric regions. *R2O* is able to find such regions by imposing a segmentation bottleneck in the form of the number of clusters, K , used in our mask prediction step. As pretraining enters the later epochs, the value of K is low, forcing the mask prediction module to segment the input image into a few larger regions using the similarity between representations for various smaller regions in the image. The transfer performance of *R2O* after ImageNet pretraining and COCO pretraining demonstrate the effectiveness of this object discovery bottleneck, as it can handle both object-centric and scene-centric data.

Limitations. While our experiments and ablations indicate that *R2O* learns object-centric masks throughout pretraining, we cannot guarantee that such masks will necessarily identify objects. As shown by the examples in the Appendix, there are several failure cases where *R2O* segmentations group different objects together or separates parts of objects that have significantly different color, texture, or brightness compared to the rest of the object. *R2O* is an unsupervised pretraining algorithm, and without semantic grounding from object-level annotations, it cannot necessarily distinguish between the semantics of what constitutes an object. Nevertheless, as indicated by our strong experimental results, *R2O* learns useful representations that can be finetuned for dense downstream prediction tasks.

5. Conclusion

We present Region-to-Object Representation Learning (*R2O*) which unifies region-based and object-centric pre-training by learning both region-level and object-centric representations using predicted masks which begin by clustering small-scale image regions and gradually progress to segment object-centric regions. While existing methods have either focused exclusively on region-based or object-centric pretraining, *R2O* shows that a region-to-object curriculum which transitions between these two objectives leads to state-of-the-art performance on a variety of downstream tasks.

References

- [1] Radhakrishna Achanta, Appu Shaji, Kevin Smith, Aurelien Lucchi, Pascal Fua, and Sabine Süsstrunk. Slic superpixels compared to state-of-the-art superpixel methods. *IEEE transactions on pattern analysis and machine intelligence*, 34(11):2274–2282, 2012. 3, 4, 13
- [2] Amir Bar, Xin Wang, Vadim Kantorov, Colorado J Reed, Roei Herzig, Gal Chechik, Anna Rohrbach, Trevor Darrell, and Amir Globerson. Detreg: Unsupervised pretraining with region priors for object detection. *arXiv preprint arXiv:2106.04550*, 2021. 2, 3
- [3] Yoshua Bengio, Aaron Courville, and Pascal Vincent. Representation learning: A review and new perspectives. *IEEE transactions on pattern analysis and machine intelligence*, 35(8):1798–1828, 2013. 2
- [4] Yaniv Benny and Lior Wolf. Onegan: Simultaneous unsupervised learning of conditional image generation, foreground segmentation, and fine-grained clustering. In *European Conference on Computer Vision*, pages 514–530. Springer, 2020. 7
- [5] Adam Bielski and Paolo Favaro. Emergence of object segmentation in perturbed generative models. *Advances in Neural Information Processing Systems*, 32, 2019. 7
- [6] Mathilde Caron, Hugo Touvron, Ishan Misra, Hervé Jégou, Julien Mairal, Piotr Bojanowski, and Armand Joulin. Emerging properties in self-supervised vision transformers. In *Proceedings of the IEEE/CVF International Conference on Computer Vision*, pages 9650–9660, 2021. 1, 2, 14
- [7] Mickaël Chen, Thierry Artières, and Ludovic Denoyer. Unsupervised object segmentation by redrawing. *Advances in neural information processing systems*, 32, 2019. 7
- [8] Ting Chen, Simon Kornblith, Mohammad Norouzi, and Geoffrey Hinton. A simple framework for contrastive learning of visual representations. In *International conference on machine learning*, pages 1597–1607. PMLR, 2020. 1, 2, 14
- [9] Xinlei Chen, Haoqi Fan, Ross Girshick, and Kaiming He. Improved baselines with momentum contrastive learning. *arXiv preprint arXiv:2003.04297*, 2020. 6, 7, 14
- [10] Xinlei Chen and Kaiming He. Exploring simple siamese representation learning. In *Proceedings of the IEEE/CVF Conference on Computer Vision and Pattern Recognition*, pages 15750–15758, 2021. 2
- [11] Xinlei Chen, Saining Xie, and Kaiming He. An empirical study of training self-supervised vision transformers. In *Proceedings of the IEEE/CVF International Conference on Computer Vision*, pages 9640–9649, 2021. 14
- [12] Jang Hyun Cho, Utkarsh Mall, Kavita Bala, and Bharath Hariharan. Picie: Unsupervised semantic segmentation using invariance and equivariance in clustering. In *Proceedings of the IEEE/CVF Conference on Computer Vision and Pattern Recognition*, pages 16794–16804, 2021. 3, 4
- [13] Dorin Comaniciu and Peter Meer. Robust analysis of feature spaces: Color image segmentation. In *Proceedings of IEEE computer society conference on computer vision and pattern recognition*, pages 750–755. IEEE, 1997. 3
- [14] Dorin Comaniciu and Peter Meer. Mean shift analysis and applications. In *Proceedings of the seventh IEEE inter-*

- national conference on computer vision*, volume 2, pages 1197–1203. IEEE, 1999. 3
- [15] MMSegmentation Contributors. MMSegmentation: Openmmlab semantic segmentation toolbox and benchmark. <https://github.com/open-mmlab/mms Segmentation>, 2020. 6, 13
- [16] Marius Cordts, Mohamed Omran, Sebastian Ramos, Timo Rehfeld, Markus Enzweiler, Rodrigo Benenson, Uwe Franke, Stefan Roth, and Bernt Schiele. The cityscapes dataset for semantic urban scene understanding. In *Proceedings of the IEEE conference on computer vision and pattern recognition*, pages 3213–3223, 2016. 5
- [17] Nameirakpam Dhanachandra, Khumanthem Manglem, and Yambem Jina Chanu. Image segmentation using k-means clustering algorithm and subtractive clustering algorithm. *Procedia Computer Science*, 54:764–771, 2015. 3
- [18] Carl Doersch, Abhinav Gupta, and Alexei A Efros. Unsupervised visual representation learning by context prediction. In *Proceedings of the IEEE international conference on computer vision*, pages 1422–1430, 2015. 2
- [19] Alexey Dosovitskiy, Lucas Beyer, Alexander Kolesnikov, Dirk Weissenborn, Xiaohua Zhai, Thomas Unterthiner, Mostafa Dehghani, Matthias Minderer, Georg Heigold, Sylvain Gelly, et al. An image is worth 16x16 words: Transformers for image recognition at scale. *arXiv preprint arXiv:2010.11929*, 2020. 5, 14
- [20] Mark Everingham, Luc Van Gool, Christopher KI Williams, John Winn, and Andrew Zisserman. The pascal visual object classes (voc) challenge. *International journal of computer vision*, 88(2):303–338, 2010. 5
- [21] Pedro F Felzenszwalb and Daniel P Huttenlocher. Efficient graph-based image segmentation. *International journal of computer vision*, 59(2):167–181, 2004. 3
- [22] Shang-Hua Gao, Zhong-Yu Li, Ming-Hsuan Yang, Ming-Ming Cheng, Junwei Han, and Philip Torr. Large-scale unsupervised semantic segmentation. *arXiv preprint arXiv:2106.03149*, 2021. 15
- [23] Spyros Gidaris, Praveer Singh, and Nikos Komodakis. Unsupervised representation learning by predicting image rotations. *arXiv preprint arXiv:1803.07728*, 2018. 2
- [24] Priya Goyal, Dhruv Mahajan, Abhinav Gupta, and Ishan Misra. Scaling and benchmarking self-supervised visual representation learning. In *Proceedings of the IEEE/CVF International Conference on computer vision*, pages 6391–6400, 2019. 13
- [25] Jean-Bastien Grill, Florian Strub, Florent Altché, Corentin Tallec, Pierre Richemond, Elena Buchatskaya, Carl Doersch, Bernardo Avila Pires, Zhaohan Guo, Mohammad Gheshlaghi Azar, et al. Bootstrap your own latent—a new approach to self-supervised learning. *Advances in Neural Information Processing Systems*, 33:21271–21284, 2020. 1, 2, 4, 6, 7, 13, 14
- [26] Kaiming He, Xinlei Chen, Saining Xie, Yanghao Li, Piotr Dollár, and Ross Girshick. Masked autoencoders are scalable vision learners. *arXiv preprint arXiv:2111.06377*, 2021. 1
- [27] Kaiming He, Xinlei Chen, Saining Xie, Yanghao Li, Piotr Dollár, and Ross Girshick. Masked autoencoders are scalable vision learners. In *Proceedings of the IEEE/CVF Conference on Computer Vision and Pattern Recognition*, pages 16000–16009, 2022. 14
- [28] Kaiming He, Haoqi Fan, Yuxin Wu, Saining Xie, and Ross Girshick. Momentum contrast for unsupervised visual representation learning. In *Proceedings of the IEEE/CVF conference on computer vision and pattern recognition*, pages 9729–9738, 2020. 1, 2, 6, 13
- [29] Kaiming He, Georgia Gkioxari, Piotr Dollár, and Ross Girshick. Mask r-cnn. In *Proceedings of the IEEE international conference on computer vision*, pages 2961–2969, 2017. 5, 13
- [30] Kaiming He, Xiangyu Zhang, Shaoqing Ren, and Jian Sun. Deep residual learning for image recognition. In *Proceedings of the IEEE conference on computer vision and pattern recognition*, pages 770–778, 2016. 5
- [31] Olivier J Hénaff, Skanda Koppula, Jean-Baptiste Alayrac, Aaron van den Oord, Oriol Vinyals, and João Carreira. Efficient visual pretraining with contrastive detection. In *Proceedings of the IEEE/CVF International Conference on Computer Vision*, pages 10086–10096, 2021. 2, 3, 6, 7, 8, 13, 14
- [32] Olivier J Hénaff, Skanda Koppula, Evan Shelhamer, Daniel Zoran, Andrew Jaegle, Andrew Zisserman, João Carreira, and Relja Arandjelović. Object discovery and representation networks. *arXiv preprint arXiv:2203.08777*, 2022. 15
- [33] Jian Hou, Huijun Gao, and Xuelong Li. Dsets-dbscan: A parameter-free clustering algorithm. *IEEE Transactions on Image Processing*, 25(7):3182–3193, 2016. 3
- [34] Jyh-Jing Hwang, Stella X Yu, Jianbo Shi, Maxwell D Collins, Tien-Ju Yang, Xiao Zhang, and Liang-Chieh Chen. Segsort: Segmentation by discriminative sorting of segments. In *Proceedings of the IEEE/CVF International Conference on Computer Vision*, pages 7334–7344, 2019. 3, 4
- [35] Sergey Ioffe and Christian Szegedy. Batch normalization: Accelerating deep network training by reducing internal covariate shift. In *Proceedings of the 32nd International Conference on Machine Learning*, Proceedings of Machine Learning Research. PMLR, 2015. 5
- [36] Xu Ji, Joao F Henriques, and Andrea Vedaldi. Invariant information clustering for unsupervised image classification and segmentation. In *Proceedings of the IEEE/CVF International Conference on Computer Vision*, pages 9865–9874, 2019. 3, 4
- [37] Asako Kanezaki. Unsupervised image segmentation by backpropagation. In *2018 IEEE international conference on acoustics, speech and signal processing (ICASSP)*, pages 1543–1547. IEEE, 2018. 3, 4
- [38] Tsung-Yi Lin, Michael Maire, Serge Belongie, James Hays, Pietro Perona, Deva Ramanan, Piotr Dollár, and C Lawrence Zitnick. Microsoft coco: Common objects in context. In *European conference on computer vision*, pages 740–755. Springer, 2014. 5
- [39] Stuart Lloyd. Least squares quantization in pcm. *IEEE transactions on information theory*, 28(2):129–137, 1982. 4
- [40] Jonathan Long, Evan Shelhamer, and Trevor Darrell. Fully convolutional networks for semantic segmentation. In *Pro-*

- ceedings of the IEEE conference on computer vision and pattern recognition*, pages 3431–3440, 2015. 6, 13
- [41] Ilya Loshchilov and Frank Hutter. Decoupled weight decay regularization. *arXiv preprint arXiv:1711.05101*, 2017. 14
- [42] Sébastien Marcel and Yann Rodriguez. Torchvision the machine-vision package of torch. In *Proceedings of the 18th ACM international conference on Multimedia*, pages 1485–1488, 2010. 13
- [43] Luke Melas-Kyriazi, Christian Rupprecht, Iro Laina, and Andrea Vedaldi. Finding an unsupervised image segmenter in each of your deep generative models. *arXiv preprint arXiv:2105.08127*, 2021. 7
- [44] Ishan Misra and Laurens van der Maaten. Self-supervised learning of pretext-invariant representations. In *Proceedings of the IEEE/CVF Conference on Computer Vision and Pattern Recognition*, pages 6707–6717, 2020. 2
- [45] Mehdi Noroozi and Paolo Favaro. Unsupervised learning of visual representations by solving jigsaw puzzles. In *European conference on computer vision*, pages 69–84. Springer, 2016. 2
- [46] Pedro O O Pinheiro, Amjad Almahairi, Ryan Benmalek, Florian Golemo, and Aaron C Courville. Unsupervised learning of dense visual representations. *Advances in Neural Information Processing Systems*, 33:4489–4500, 2020. 2, 3
- [47] Aaron van den Oord, Yazhe Li, and Oriol Vinyals. Representation learning with contrastive predictive coding. *arXiv preprint arXiv:1807.03748*, 2018. 2
- [48] Adam Paszke, Sam Gross, Francisco Massa, Adam Lerer, James Bradbury, Gregory Chanan, Trevor Killeen, Zeming Lin, Natalia Gimelshein, Luca Antiga, Alban Desmaison, Andreas Kopf, Edward Yang, Zachary DeVito, Martin Raison, Alykhan Tejani, Sasank Chilamkurthy, Benoit Steiner, Lu Fang, Junjie Bai, and Soumith Chintala. Pytorch: An imperative style, high-performance deep learning library. In H. Wallach, H. Larochelle, A. Beygelzimer, F. d’Alché-Buc, E. Fox, and R. Garnett, editors, *Advances in Neural Information Processing Systems 32*, pages 8024–8035. Curran Associates, Inc., 2019. 5
- [49] Colorado J Reed, Sean Metzger, Aravind Srinivas, Trevor Darrell, and Kurt Keutzer. Selfaugment: Automatic augmentation policies for self-supervised learning. In *Proceedings of the IEEE/CVF Conference on Computer Vision and Pattern Recognition (CVPR)*, pages 2674–2683, June 2021. 2
- [50] Olaf Ronneberger, Philipp Fischer, and Thomas Brox. U-net: Convolutional networks for biomedical image segmentation. In *International Conference on Medical image computing and computer-assisted intervention*, pages 234–241. Springer, 2015. 7
- [51] Olga Russakovsky, Jia Deng, Hao Su, Jonathan Krause, Sanjeev Satheesh, Sean Ma, Zhiheng Huang, Andrej Karpathy, Aditya Khosla, Michael Bernstein, et al. Imagenet large scale visual recognition challenge. *International journal of computer vision*, 115(3):211–252, 2015. 5
- [52] Ramprasaath R Selvaraju, Karan Desai, Justin Johnson, and Nikhil Naik. Casting your model: Learning to localize improves self-supervised representations. In *Proceedings of the IEEE/CVF Conference on Computer Vision and Pattern Recognition*, pages 11058–11067, 2021. 2, 3
- [53] Yonglong Tian, Dilip Krishnan, and Phillip Isola. Contrastive multiview coding. *arXiv preprint arXiv:1906.05849*, 2019. 8
- [54] Jasper RR Uijlings, Koen EA Van De Sande, Theo Gevers, and Arnold WM Smeulders. Selective search for object recognition. *International journal of computer vision*, 104(2):154–171, 2013. 3, 7, 15
- [55] Wouter Van Gansbeke, Simon Vandenhende, Stamatios Georgoulis, and Luc V Gool. Revisiting contrastive methods for unsupervised learning of visual representations. *Advances in Neural Information Processing Systems*, 34:16238–16250, 2021. 6
- [56] Wouter Van Gansbeke, Simon Vandenhende, Stamatios Georgoulis, Marc Proesmans, and Luc Van Gool. Scan: Learning to classify images without labels. In *European conference on computer vision*, pages 268–285. Springer, 2020. 4
- [57] Wouter Van Gansbeke, Simon Vandenhende, Stamatios Georgoulis, and Luc Van Gool. Unsupervised semantic segmentation by contrasting object mask proposals. In *Proceedings of the IEEE/CVF International Conference on Computer Vision*, pages 10052–10062, 2021. 2, 3
- [58] Andrey Voynov, Stanislav Morozov, and Artem Babenko. Object segmentation without labels with large-scale generative models. In *International Conference on Machine Learning*, pages 10596–10606. PMLR, 2021. 7
- [59] Catherine Wah, Steve Branson, Peter Welinder, Pietro Perona, and Serge Belongie. The caltech-ucsd birds-200-2011 dataset. 2011. 5
- [60] Xinlong Wang, Rufeng Zhang, Chunhua Shen, Tao Kong, and Lei Li. Dense contrastive learning for self-supervised visual pre-training. In *Proceedings of the IEEE/CVF Conference on Computer Vision and Pattern Recognition*, pages 3024–3033, 2021. 2, 3, 6, 7, 14
- [61] Fangyun Wei, Yue Gao, Zhirong Wu, Han Hu, and Stephen Lin. Aligning pretraining for detection via object-level contrastive learning. *Advances in Neural Information Processing Systems*, 34, 2021. 3
- [62] Xin Wen, Bingchen Zhao, Anlin Zheng, Xiangyu Zhang, and Xiaojuan Qi. Self-supervised visual representation learning with semantic grouping. *arXiv preprint arXiv:2205.15288*, 2022. 3, 6, 7, 14
- [63] Yuxin Wu, Alexander Kirillov, Francisco Massa, Wan-Yen Lo, and Ross Girshick. Detectron2. <https://github.com/facebookresearch/detectron2>, 2019. 5
- [64] Tete Xiao, Colorado J Reed, Xiaolong Wang, Kurt Keutzer, and Trevor Darrell. Region similarity representation learning. In *Proceedings of the IEEE/CVF International Conference on Computer Vision*, pages 10539–10548, 2021. 2, 3, 6, 14
- [65] Enze Xie, Jian Ding, Wenhai Wang, Xiaohang Zhan, Hang Xu, Peize Sun, Zhenguo Li, and Ping Luo. Detco: Unsupervised contrastive learning for object detection. In *Proceedings of the IEEE/CVF International Conference on Computer Vision*, pages 8392–8401, 2021. 3, 6, 14
- [66] Jiahao Xie, Xiaohang Zhan, Ziwei Liu, Yew Soon Ong, and Chen Change Loy. Unsupervised object-level representation

- learning from scene images. *Advances in Neural Information Processing Systems*, 34:28864–28876, 2021. 2, 3, 4, 6
- [67] Zhenda Xie, Yutong Lin, Zheng Zhang, Yue Cao, Stephen Lin, and Han Hu. Propagate yourself: Exploring pixel-level consistency for unsupervised visual representation learning. In *Proceedings of the IEEE/CVF Conference on Computer Vision and Pattern Recognition*, pages 16684–16693, 2021. 2, 3, 6, 14
- [68] Yufei Xu, Qiming Zhang, Jing Zhang, and Dacheng Tao. Regioncl: Can simple region swapping contribute to contrastive learning? *arXiv preprint arXiv:2111.12309*, 2021. 2, 3
- [69] Chenhongyi Yang, Lichao Huang, and Elliot J Crowley. Contrastive object-level pre-training with spatial noise curriculum learning. *arXiv preprint arXiv:2111.13651*, 2021. 2, 3
- [70] Yang You, Igor Gitman, and Boris Ginsburg. Scaling sgd batch size to 32k for imagenet training. *arXiv preprint arXiv:1708.03888*, 6(12):6, 2017. 13
- [71] Feihu Zhang, Philip Torr, Rene Ranftl, and Stephan Richter. Looking beyond single images for contrastive semantic segmentation learning. *Advances in Neural Information Processing Systems*, 34, 2021. 4
- [72] Richard Zhang, Phillip Isola, and Alexei A Efros. Colorful image colorization. In *European conference on computer vision*, pages 649–666. Springer, 2016. 2

Appendix

A.1. Pretraining Details

Data Augmentation We follow the BYOL [25] data augmentation pipeline. SLIC [1] masks are generated using a resized (224×224) copy of the input image. To generate the augmented views, we implement the following operations using torchvision [42].

1. Random Crop: Generate two distinct random crops from the original image. Afterwards we resize both views to 224×224 .
2. Horizontal Flip: We flip the views horizontally with a 0.5 probability.
3. Color Jitter: With an implementation probability of 0.8 we set brightness equal to 0.4, contrast = 0.4, saturation = 0.2 and hue = 0.1.
4. Grayscale: We convert the images from RGB to Grayscale with a 0.2 probability.
5. Gaussian Blur: We always apply blurring for the first view and with a 0.1 probability for the second view. We use a 23×23 kernel with a standard deviation chosen uniformly at random between ranges $[0.1, 2.0]$.
6. Solarize: Solarize only implemented on view 2 with a probability of 0.2 using the PIL package and a threshold of 128.

Mask Prediction We employ a cosine schedule for the number of segments, K , which starts at K_0 at epoch 0 and gradually decreases to K_f between epoch t_α and T_{epoch} , where T_{epoch} is the total number of epochs during the pretraining. Equation (A1) expresses K as a function of t , the epoch number. We choose $K_0 = 128, K_f = 4$ in our experiments. We set $t_\alpha = 40$ during ImageNet-1K and ImageNet-100 pretraining and set $t_\alpha = 8$ during COCO pretraining.

$$K(t) = \begin{cases} K_0, & \text{if } t < t_\alpha \\ K_f + \cos\left(\frac{2(t-t_\alpha)}{(T_{epoch}-t_\alpha)\cdot\pi}\right)(K_0 - K_f) & \text{otherwise} \end{cases} \quad (\text{A1})$$

Optimization We followed the optimization details of BYOL [25]. The online network is updated by a LARS optimizer [70] with a base learning rate of 0.3 and a weight decay of 10^{-6} . The actual maximum learning rate during training is $\text{base_lr} \times \frac{\text{global_batch_size}}{256} \times K_0$. The learning rate increases linearly during the warmup period and then decreases following a cosine schedule. Throughout

training, the learning rate is scaled by $K(t)$. In our experiment, the global batch size is 4096 and the warmup period is 3 epochs. The target network parameter ξ is updated by $\xi^t \leftarrow (1 - \tau^t) \cdot \theta^t + \tau^t \cdot \xi^{t-1}$ where θ is the online network parameter and τ increases from 0.99 to 1.00 following a cosine schedule.

A.2. Transfer Learning Details

Object Detection and Instance Segmentation: MS COCO We adopt Mask-RCNN [29] architecture with a ResNet-50 backbone and FPN. In the fine tuning stage, images are randomly flipped and resized to $u \cdot 1024$ on the longest side where u is uniformly sampled in $[0.8, 1.25]$. The images are then padded or cropped to 1024×1024 . The aspect ratio is kept the same as original image. During the evaluation, the images are resized to 1024 on the longest side. We finetune on COCO for the $1 \times$ (12 epochs) and $2 \times$ (24 epochs) schedule using stochastic gradient descent. We swept between learning rates of 0.003, 0.1, 0.3 for our model and our DetCon [31] implementation to ensure a fair comparison. We use a momentum of 0.9, a weight decay of $4 \cdot 10^{-5}$, and a global batch size of 32. The learning rate increases linearly in the first 1000 epochs and drops twice by a factor of 10 after $\frac{2}{3}$ and $\frac{8}{9}$ of the total training time.

Semantic Segmentation: PASCAL VOC and Cityscapes

We adopt FCN [40] architecture with a ResNet-50 backbone. We made the following architecture changes on the backbone according to MOCO [28]. The 3×3 convolutions in conv5 blocks have dilation 2 and stride 1. This is followed by two extra 3×3 convolutions of 256 channels with BN and ReLU, and then a 1×1 convolution for per-pixel classification. We set dilation = 6 in the two extra 3×3 convolutions. All other implementation details are the default of MMSegmentation [15]. For PASCAL VOC, we fine tuned on train_aug2012 and evaluated on val2012 dataset. The images are randomly flipped, scaled by a ratio randomly sampled in $[0.5, 2.0]$, and then cropped to 513×513 during the training. The evaluation is performed on the original image size. We fine tuned for 30k iterations with a batch size of 16 and a weight decay of 10^{-4} . The learning rate is dropped by a factor of 10 at $\frac{7}{10}$ and $\frac{9}{10}$ of the total training time. For Cityscapes, we fine tuned on train_fine and evaluated on val_fine dataset. The images are randomly flipped, resized to 2049×1025 , scaled by a ratio randomly sampled in $[0.5, 2.0]$, and then cropped to 769×769 during the training. The evaluation is performed on a resolution of 2049×1025 . We fine tuned for 30k iterations with a batch size of 16, and a weight decay of 10^{-4} . The learning rate is dropped by a factor of 10 at $\frac{7}{10}$ and $\frac{9}{10}$ of the total training time. To ensure a fair comparison, we followed the practice of [24] and evaluate each pretraining method under a variety of learning rates and report the best results. We also

report the standard deviation across three random seeds. For PASCAL VOC, we swept between the learning rate 0.001, 0.003, 0.01, 0.03, 0.1. For Cityscapes, we swept between learning rate 0.004, 0.01, 0.04.

A.3. Extended Experimental Results

We conduct additional experiments and report the average performance on semantic segmentation and instance detection/segmentation with standard deviation across 3 different seeds in Table 5 and Table 6.

Method	PASCAL VOC	Cityscapes
Supervised	72.4	74.7
MoCo v2 [9]	73.9 ± 0.12	75.6 ± 0.09
BYOL [†] [25]	75.0 ± 0.22	75.8 ± 0.31
DenseCL [60]	73.8 ± 0.2	76.1 ± 0.12
DetCon _B [†] [31]	76.0 ± 0.14	76.2 ± 0.09
ReSim [64]	74.3 ± 0.28	75.5 ± 0.15
PixPro [67]	74.2 ± 0.44	75.9 ± 0.37
DetCo [65]	74.3 ± 0.07	74.9 ± 0.46
SlotCon [62]	76.2 ± 0.24	76.1 ± 0.19
<i>R2O</i>	77.2 ± 0.15	76.9 ± 0.38

Table 5. Performance on PASCAL VOC and Cityscapes semantic segmentation (mIOU) with standard deviation across 3 seeds. [†]: Results from re-implementation of pretraining method.

Method	Epochs	AP ^{bb}	AP ^{mk}
BYOL [†]	300	40.3 (± 0.10)	37.5 (± 0.08)
DetCon _B [†]	300	41.5 (± 0.03)	38.0 (± 0.09)
<i>R2O</i>	300	41.7 (± 0.02)	38.3 (± 0.07)

Table 6. Performance on COCO object detection and instance segmentation with standard deviation following the 1× schedule averaged across 3 seeds. [†]: Results from re-implementation.

A.4. Exploring Contrastive Representation Learning

We investigate using a contrastive objective function for L_{repr} . We follow the authors of SimCLR [8] and use the NT-Xent objective and employ the same architecture, data augmentation policy, and optimization details. We adopt the mask sampling strategy employed by DetCon [31] in order to reduce the memory overhead caused by the cross-GPU gather operation used in contrastive learning. Table 7 compares the performance when using the SimCLR objective or the BYOL objective. Both methods were pre-trained on ImageNet-100 using the default region-to-object ($K = 128 \rightarrow K = 4$) schedule. The BYOL objective leads to an improvement of +4.51 on PASCAL and +1.44

Objective	PASCAL VOC	Cityscapes
SimCLR NT-Xent	62.99 ± 0.02	69.99 ± 0.17
BYOL	67.5 ± 0.1	71.43 ± 0.25

Table 7. Comparing contrastive and Siamese representation learning objectives. We investigate using contrastive learning, via the Simclr NT-Xent objective, during *R2O* pretraining. We find that using a Siamese representation learning objective such as BYOL outperforms its contrastive counterpart when finetuned for PASCAL VOC (+4.51) and Cityscapes (+1.44) semantic segmentation. Results report mean intersection-over-union (mIOU).

Method	AP ^{bb}	AP ^{mk}
MAE [27]	34.8	31.7
<i>R2O</i>	40.5	36.6

Table 8. Examining COCO object detection and instance segmentation performance when pretraining a ViT. We report Average Precision on bounding box (AP^{bb}) and mask (AP^{mk}) predictions for val2017 after pretraining on ImageNet-100 for 300 epochs.

on Cityscapes for the task of semantic segmentation. We note that the authors of DetCon [31] demonstrated similar results when using a contrastive objective, with DetCon_S requiring up to 3 times the pretraining in order to match the performance of DetCon_B.

A.5. Exploring Vision Transformer Architectures

Inspired by the recent progress in applications of Vision Transformer (ViT) architectures [6, 11, 19, 27], we experiment with applying *R2O* pretraining to a ViT-Base (ViT-B) architecture. We apply additional transpose convolution layers during the pretraining on the feature maps in the final transformer block to get 7x7 and 14x14 feature maps to mimic the output of ResNet C5 and C4 output. We did not make any other changes to the architecture or the loss. We pretrained *R2O* and MAE for 300 epochs on ImageNet-100 with a global batch size of 1024. We used the exact same optimization set up as our ResNet experiments. The base learning rate is 0.3 following a cosine decay schedule. The momentum is 0.9 and weight decay is 10^{-6} . For MAE, we strictly followed the optimization settings written in the paper [27]. We evaluate the pretrained weights on MS COCO for the task of object detection and instance segmentation. We finetuned for 1× schedule (12 epoch) using AdamW optimizer [41]. The learning rate is 3e-4, the layer-wise decay rate is 0.75, and the drop path rate is 0.2. The learning rate is multiplied by 0.1 at epochs 9 and 11. Table 8 compares MAE [27] to *R2O* when using a ViT-B encoder af-

Curriculum	PASCAL VOC	ImageNet-100
16	68.7	76.3
64	68.8	75.7
160	69.2	73.9
4 \rightarrow 16	63.1	63.8
4 \rightarrow 64	69.1	75.1
4 \rightarrow 128	69.1	80.0
16 \rightarrow 4	67.5	73.8
64 \rightarrow 4	71.8	84.4
128 \rightarrow 4	72.1	85.5

Table 9. **Comparing fixed K , object-to-region, and region-to-object curriculums.** We pretrain an encoder on ImageNet-100 while using alternate schedules for our mask prediction step. We report mean intersection-over-union (mIOU) on PASCAL VOC semantic segmentation and ImageNet-100 k -NN accuracy (%). We refer to any K schedule which starts from a low number and ends at a high number, *e.g.* $K = 4 \rightarrow K = 128$, as object-to-region.

ter pretraining on ImageNet-100 for 300 epochs. The $R2O$ pretrained encoder provides a +5.7 increase in AP^{bb} and a +4.9 increase in AP^{mk} relative to MAE. Thus, the benefits of $R2O$ pretraining for dense prediction tasks also apply to newer architectures such as ViTs.

Evaluating Alternate Curriculums. Table 9 demonstrates that a region-to-object curriculum leads to the best transfer performance on PASCAL VOC (+2.9 mIOU) for semantic segmentation and for ImageNet-100 k -NN classification (+5.5%). This schedule outperforms using a fixed K and an opposite curriculum which increases K from a low value to a high value. Using a fixed K does not allow for learning both region based features and object centric representation learning. If the fixed value of K is high, say $K = 64$, then refined masks will have many distinct regions and the representation learning step will train features corresponding to small image regions or object parts. A small fixed value of K , say $K = 4$, has the opposite effect as representations learned will simply match large image regions across views and cannot learn small region based features necessary for pixel level prediction tasks. The opposite curriculum, denoted as object-to-region, also leads to suboptimal performance. We believe this is because such a schedule does not allow for objects to be found and represented. Instead, early refined masks are just large image regions which lack semantic meaning as the network has undergone very little training.

A.6. Impact of Scheduler Type

We also experiment with the type of region-to-object scheduler. The cosine scheduler, which was used in our ImageNet-1K and COCO pretraining experiments, performs similarly to the linear scheduler on PASCAL VOC semantic segmentation (72.1 mIOU cosine scheduler versus 72.2 mIOU linear scheduler) and ImageNet-100 k -NN classification (85.5% cosine scheduler versus 85.2% linear scheduler) after pretraining on ImageNet-100. This result shows the benefit of region-to-object pretraining as similar performance can be achieved regardless of the type of scheduler used during pretraining.

A.7. Importance of Region-Level Prior

We further compare using the SLIC region-level prior with a spatial heuristic which divides the image into 14×14 square patches. We find that both priors lead to similar performance on PASCAL VOC segmentation (72.1 mIOU SLIC versus 72.7 mIOU spatial), but using a SLIC prior leads to a larger, more significant difference (+2.5%) in ImageNet-100 k -NN accuracy (85.5% SLIC versus 83.0% spatial). This suggests that using a broader set of image-level criteria, *e.g.* color resemblance and spatial proximity in the case of SLIC, to generate our region-level prior will improve downstream transfer performance.

A.8. Quantifying the objectness of masks throughout pre-training.

We use the Average Best Overlap (ABO) [54] to measure the improvement of masks throughout training using semantic segmentation annotations for ImageNet-1K provided by LUSS [22]. As shown in Figure 4, our ABO improved by +0.25 over the course of pretraining. Figure 4 also includes the ABO of our SLIC prior as well. Masks predicted by $R2O$ are consistently better than SLIC segments, suggesting that the mask prediction step is able to improve small region priors into more semantically meaningful object-like masks

A.9. Odin Reimplementation Details

We reproduced Odin [32] using a ResNet-50 encoder. We followed the optimization details mentioned by the authors. Specifically, the learning rate is linearly scaled by global batch size and decays following a cosine schedule. We trained Odin on ImageNet-100 for 300 epochs using a global batch size of 1024 across 32 NVIDIA V100 GPUs.

A.10. Visualization of Mask Predictions

ImageNet-1K Pretraining In Figure 5, we visualize the masks generated by $R2O$ in the mask prediction step during

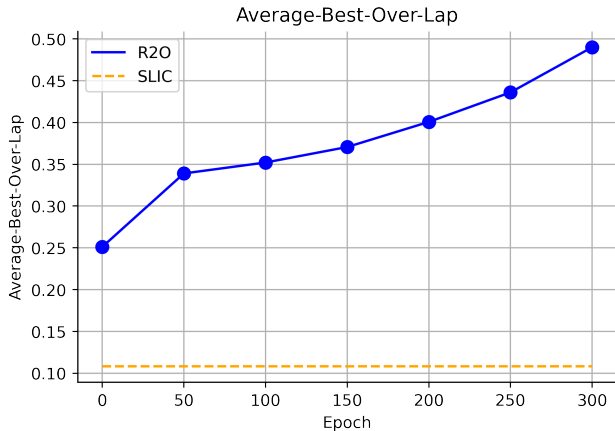


Figure 4. ***R2O* predicted masks become increasingly object-centric over pretraining.** We compute average best overlap (ABO) for ImageNet segmentations (using LUSS annotations) generated over the course of pretraining. For reference, we also display the ABO of our region-level prior (SLIC).

pretraining. The number of segments, K , starts at 128 and gradually decreases to 4 following a cosine schedule. At 100 epoch, $K = 119$. At 200 epoch, $K = 74$. At 300 epoch, $K = 4$.

In Figure 6, we visualize some failure cases where the masks failed to capture objects. In these examples, masks group pixels that are similar in color and texture but do not belong to the same object (examples 1, 3). They also tend to over-segment regions into multiple parts if those parts have large disparities in color and texture such as the background, while at the same time, ignore smaller objects (example 2). In a few extreme cases, the masks groups all the pixels in entire image as belonging to the same object (example 2). Since we are performing K-means over the batch, this could happen when there is large variance across region-level features in the batch while the variance in region-level features from the given image is small. However, even in this worst case scenario, our representation learning step amounts to using the standard BYOL objective with global-pooling.

A.11. Visualization of Caltech-UCSD Birds 200-2011 Segmentation

We also perform unsupervised segmentation on Caltech-UCSD with K-means clustering, setting $K = 5$, using *R2O* ImageNet pre-trained features. Figure 7 visualizes some of the masks.

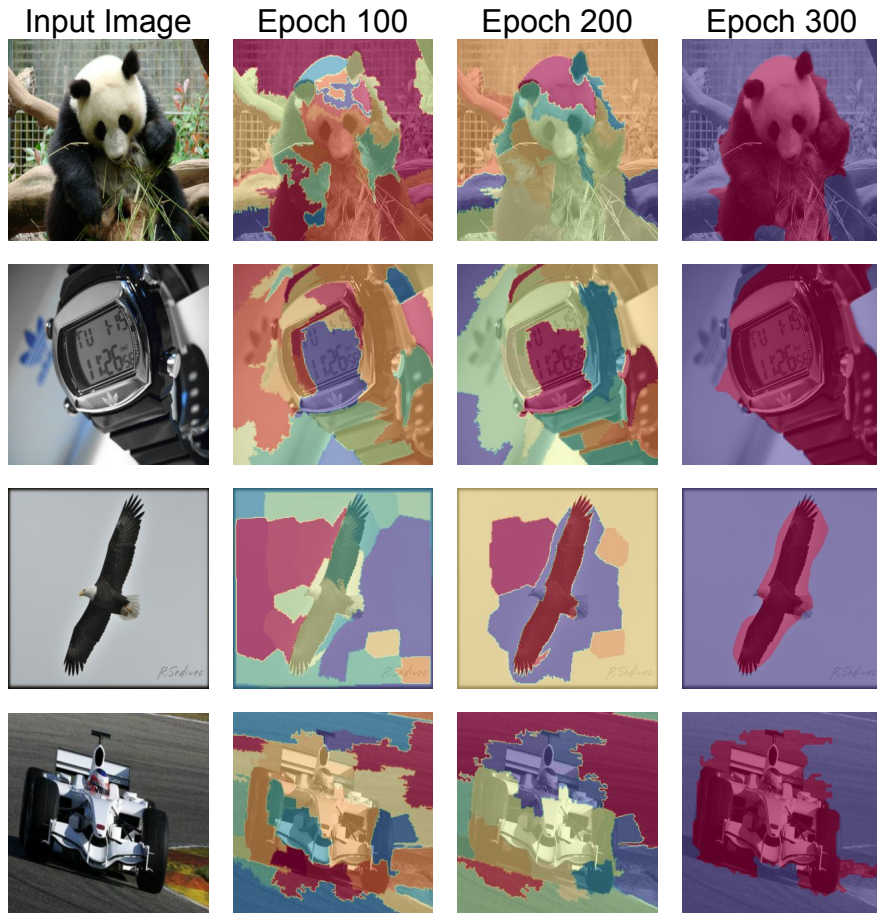


Figure 5. **Visualization of predicted masks generated during ImageNet pretraining** after 100, 200 and 300 epochs. As depicted, early masks consists of random image segments which gradually become object-centric segmentations.

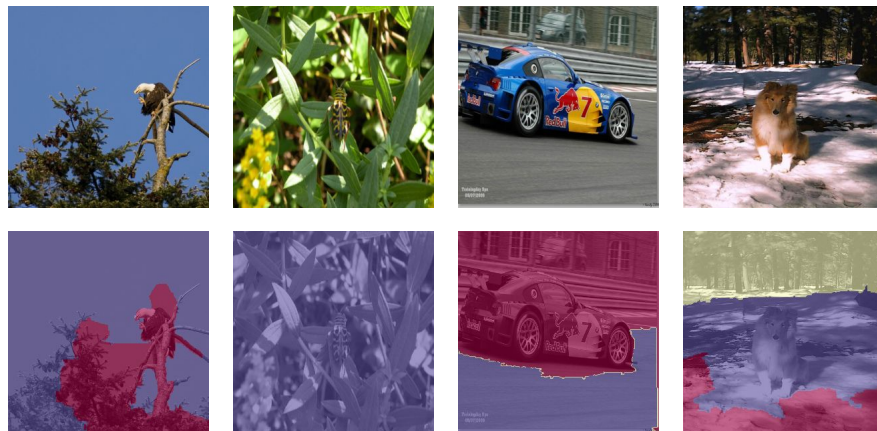


Figure 6. **Visualization of Failure Cases.** We visualize some of the poorly segmented masks generated during pretraining. From left to right: In example 1, one mask groups the eagle and part of the background together because of similar colors. In example 2, the mask is unable to detect any significant object in the image because the insect blends in the background. In examples 3 and 4, the masks focus more on the separation between the background and foreground and thus ignore the car and dog.

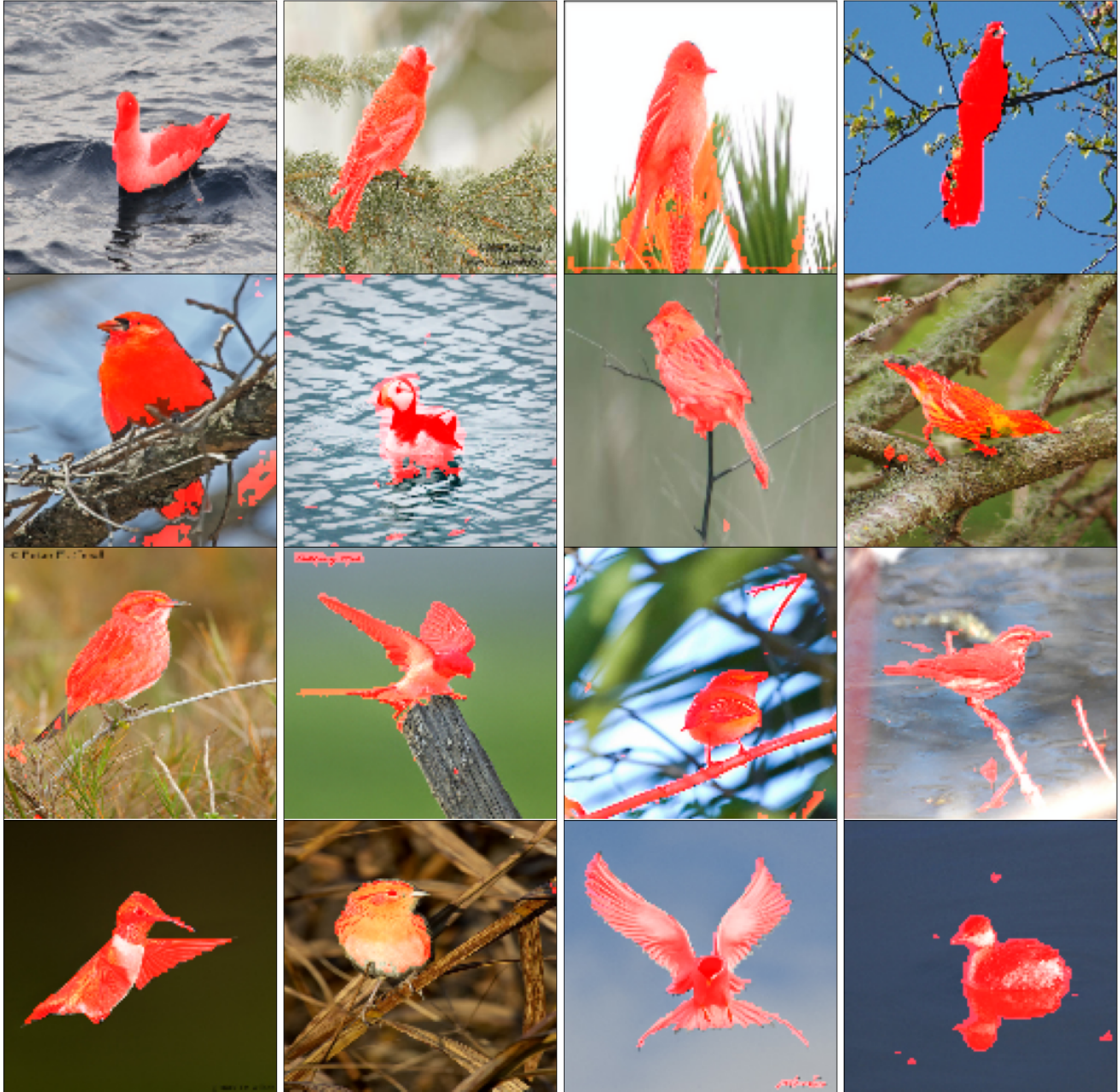


Figure 7. **Visualization of Caltech-UCSD Birds 200-2011 Segmentation.** We perform unsupervised segmentation by clustering feature representations on a per-image basis with $K = 5$. The best match is considered as the foreground.